Weather and Climate Extremes 45 (2024) 100710

Contents lists available at ScienceDirect

Weather and Climate Extremes

journal homepage: www.elsevier.com/locate/wace

The 2022-23 drought in the South American Altiplano: ENSO effects on moisture flux in the western Amazon during the pre-wet season

Ricardo A. Gutierrez-Villarreal [a,*], Jhan-Carlo Espinoza [b,c], Waldo Lavado-Casimiro [a,d], Clémentine Junquas [b,d], Jorge Molina-Carpio [e], Thomas Condom [b], José A. Marengo [f,g,h]

[a] Escuela de Posgrado, Universidad Nacional Agraria La Molina, Lima, Peru
[b] Univ. Grenoble Alpes, IRD, CNRS, INRAE, Grenoble-INP, IGE, 38000 Grenoble, France
[c] Instituto de Investigación sobre la Enseñanza de las Matemáticas, Pontificia Universidad Católica del Perú, (PUCP), Lima, Perú
[d] Servicio Nacional de Meteorología e Hidrología, Lima, Perú
[e] Universidad Mayor de San Andrés, Instituto de Hidráulica e Hidrología, La Paz, Bolivia
[f] National Center for Monitoring and Early Warning of Natural Disasters/CEMADEN, São José dos Campos, Brazil
[g] Graduate Program in Natural Disasters, UNESP/CEMADEN, São José dos Campos, Brazil
[h] Graduate School of International Studies. Korea University, Seoul, South Korea

ARTICLE INFO

Keywords:
Lake Titicaca
Desaguadero river and lake Poopó hydrological system
Drought –climate variability
El Niño Southern Oscillation
South American Altiplano

ABSTRACT

The 2022-23 hydrological year in the Lake Titicaca, Desaguadero River, and Lake Poopó hydrological system (TDPS) over the South American Altiplano constituted a historically dry period. This drought was particularly severe during the pre-wet season (October–December), when the TDPS and the adjacent Andean-Amazon region experienced as much as 60% reductions in rainfall. Consequently, Titicaca Lake water levels decreased by 0.05 m from December to January, which is part of the rising lake level period of normal conditions. Such conditions have not been seen since the El Niño-related drought of 1982-83. Using a set of hydroclimatic, Sea Surface Temperature (SST) and atmospheric reanalysis datasets, we find that this new historical drought was associated with enhanced southerly moisture flux anomalies, reducing the inflow of moisture-laden winds from the Amazon basin to the TDPS. Such anomalies in moisture transport were not seen since at least the 1950s. The atmospheric dynamics associated with this drought are related to La Niña SST anomalies via subtropical teleconnections associated with Rossby wave trains towards South America, further extended by subtropical Atlantic Ocean SST anomalies. This feature reduced the atmospheric moisture inflow from the Amazon and weakened the development of the Bolivian High in the upper troposphere. These results document a new atmospheric mechanism related to extreme droughts in the TDPS associated with La Niña SST anomalies during the pre-wet season. This goes beyond the traditional understanding of El Niño events, especially the strongest ones, being associated with dry conditions in the TDPS during the wet season (December–March).

1. Introduction

The South American Altiplano, located between the wet Amazon rainforest and Pantanal wetland at the east and the desert of Peru-Chile at the west (Fig. 1a), is characterized by frequent extreme hydroclimatological events such as floods and droughts (Arias et al., 2021; Poveda et al., 2020). In this region, below-normal precipitation events impact the Lake Titicaca, Desaguadero River, and Lake Poopó hydrological system (TDPS; Fig. 1a), significantly affecting agriculture (predominantly rainfed), cattle breeding and economical activities, as well as the proliferation of pests and diseases (UNEP, 1996; García and Alavi, 2018; Satgé et al., 2019). Thus, its population, already facing significant vulnerability to poverty, is highly prone to drought-related impacts (Sietz et al., 2012).

The annual cycle of rainfall over the TDPS exhibits a marked seasonality with a rainy season (December to March) that attains more than 75% of the annual precipitation, a dry season (May to August) and a pre-wet season (September to December) (Garreaud et al., 2003; Sedlmeier et al., 2023). The strong seasonality of rainfall in this region is related to the upper level anticyclone over the Peruvian-Bolivian Altiplano, known also as the Bolivian High (BH) during the austral summer, which enhances zonal moisture transport from the Amazon basin towards the

* Corresponding author.
E-mail address: ra.gvillarreal@gmail.com (R.A. Gutierrez-Villarreal).

https://doi.org/10.1016/j.wace.2024.100710
Received 22 January 2024; Received in revised form 20 June 2024; Accepted 28 July 2024
Available online 29 July 2024

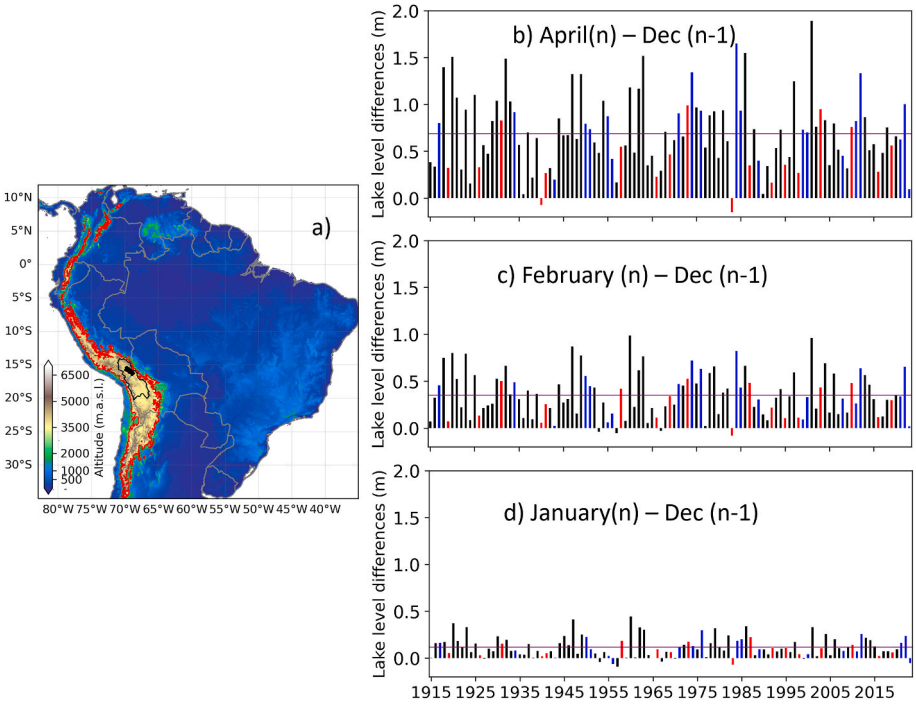

Fig. 1. Lake Titicaca's geographical location and hydrograms. a) The Lake Titicaca, Desaguadero River, and Lake Poopo basins (TDPS system) boundary is delimited by a black line, and the lake area is represented by a black polygon. Red lines in the Andean cordillera denote altitudes of 3 000 m.a.s.l. Interannual increment of lake levels of b) April, c) February, and d) January, with respect to December. The dataset spans between 1914 and 2023. The purple horizontal lines represent the long-term (1914–2023) average of lake level differences. "n" refers to the calendar year. Selected El Niño (La Niña) years are tagged with red (blue) bars if the El Niño 3.4 index from the HadiSST dataset is higher (lower) than 0.75 (−0.75) during at least 4 months between October $_{n-1}$ and April $_{n}$. (For interpretation of the references to color in this figure legend, the reader is referred to the Web version of this article.)

Altiplano and favors convection over the region (Espinoza et al., 2020). The BH is a component of the South American Monsoon System (SAMS) (Marengo et al., 2012; Vera et al., 2006). The peak of precipitation occurs in January and is characterized by intense convective activity combined with moisture advection from the Amazon Basin. During the austral winter, the moist eastern flux is replaced by westerly winds, which provide dry air linked to the atmospheric stability over the Pacific Ocean and is associated with a higher frequency of frost events (Espinoza et al., 2020; Garreaud, 2009; Segura et al., 2022; Sulca et al., 2018b). The pre-wet season synoptic climatology in the upper troposphere is consistent with a weakening of wintertime conditions and the predominance of summertime conditions (Espinoza et al., 2020).

While the rainy season is certainly more important in terms of the actual rainfall accumulation, positive (negative) rainfall anomalies during the pre-wet season can be strongly related to the anticipation (delays) of the onset of the rainy season. Delays in the onset of the rainy season can seriously affect agricultural activities and productivity; for example, by inducing i) delays in sowing and the need to re-sow due to the appearance of dry spells during the time of the normal sowing period, and ii) crop physiological stress due to water scarcity and large thermal amplitude associated with low cloudiness (Garcia et al., 2007; Geerts et al., 2006).

An enhanced convection in the central (western) Tropical Pacific during El Niño (La Niña) promotes zonal large-scale disturbances and intensity of the Walker cell, leading to increased subsidence (convergence) in equatorial South America and Amazon (Cai et al., 2020). In addition, El Niño (La Niña) leads to anomalies in the meridional Hadley cell, inducing weaker (stronger) convection in equatorial South America, and the opposite in the descending branch of the Hadley cell in the subtropics (Yoon and Zeng, 2010). Furthermore, disturbances caused by anomalous deep convection over the Tropical Pacific are able to excite extratropical Rossby wave trains that propagates via a pathway known as the Pacific-South American pattern (Karoly, 1989; Mo, 2000). All the above-mentioned ENSO-induced anomalies are able to produce moisture flux anomalies across the Amazon basin, where El Niño (La Niña) is often associated with dry (wet) conditions (Espinoza et al., 2022; Marengo and Espinoza, 2016) and an intensification (weakening) of the South American Low Level Jet (SALLJ, Jones et al., 2023; Montini et al., 2019). This atmospheric feature enhances (reduces) moisture transport towards the La Plata basin, where floods (droughts) are related to El Niño (La Niña) events (Zanin and Satyamurty, 2020).

It is worth mentioning that studies on El Niño impacts in climate variability in the TDPS have paid more attention to the wet season instead of the pre-wet season. In the Altiplano, extreme El Niño (La Niña) events have been related to drought (flood) conditions during the rainy season (Garreaud et al., 2003; Jonaitis et al., 2021; W. Lavado-Casimiro and Espinoza, 2014; Lavado-Casimiro et al., 2013; Segura et al., 2019; Sulca et al., 2018a). This relationship is more significant for the western and southern part of the TDPS rather than in the eastern region (Jonaitis et al., 2021). However, the sign of the impacts of El Niño and La Niña on precipitation is reversed during the pre-wet season of September–December (Lavado-Casimiro and Espinoza, 2014; Lavado-Casimiro et al., 2013; Sulca et al., 2018a,b). Indeed, for the September–November season, these studies documented negative rainfall anomalies in the Peruvian-Bolivian Altiplano during La Niña years. While this reversal and its impacts are documented at the regional scale for South America and Southeastern South America (De Souza et al., 2021; Kayano et al., 2021; Lopes et al., 2022), its specific mechanisms and effects on precipitation in the tropical Andes, particularly over the Altiplano region, remain to be elucidated.

SST anomalies over the subtropical southern Atlantic Ocean are also able to induce significant rainfall variability in tropical regions such as the southwestern Amazon basin; which is located immediately to the east of the TDPS (Espinoza et al., 2014). For example, during the austral summer of 2014, that region experienced rainfall anomalies about 100% above normal. Such anomalies were associated with an exceptional SST

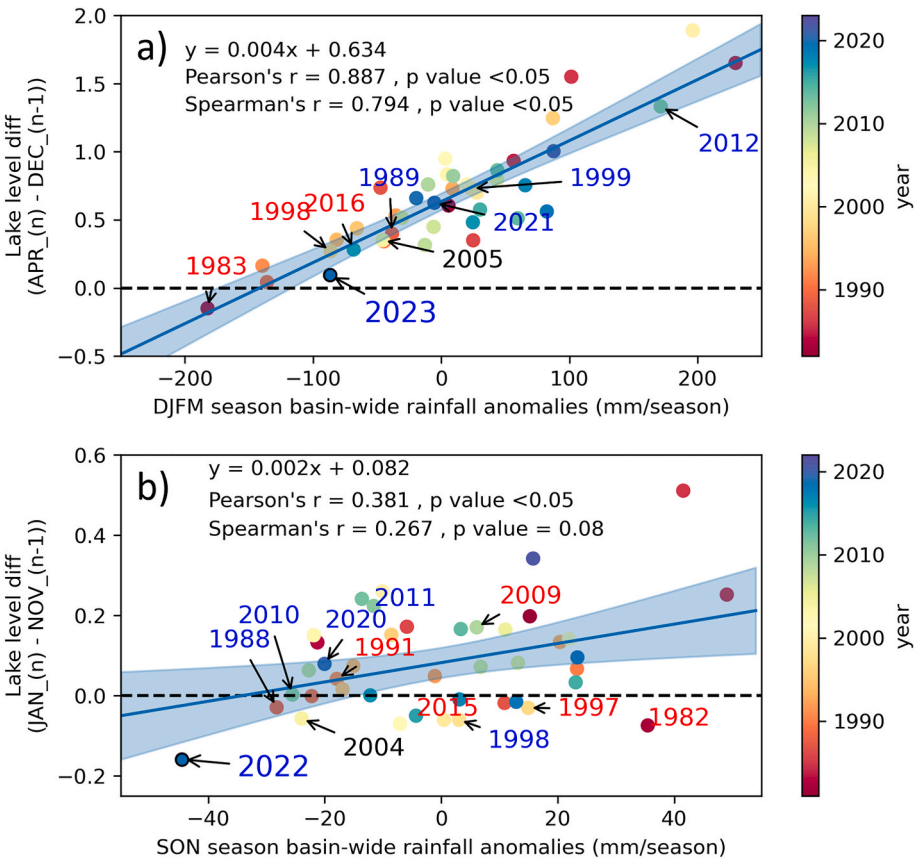

Fig. 2. TDPS-averaged rainfall control on Lake Titicaca level differences. Linear regression and scatterplot between pre-wet (a) wet season rainfall anomalies (December–March), and lake level differences between April (n) and November of previous calendar year (n-1). b) Same as a), but considering pre-wet rainfall anomalies (September–November) and lake level differences between January(n) and November of previous calendar year (n-1). Blue envelopes the linear regression line represents the 95% confidence interval. Note the differences in x and y scales. Selected El Niño (La Niña) years are colored as red (blue) if the El Niño 3.4 index from the HadiSST dataset is higher (lower) than 0.75 (−0.75) during at least 4 months between October $_{n-1}$ and April $_{n}$. (For interpretation of the references to color in this figure legend, the reader is referred to the Web version of this article.)

gradient over the subtropical South Atlantic, with important warm (cold) SST anomalies near the southern coast of Brazil (southern Argentina, this region is delimited in Figure S1 and Section 5) (Coelho et al., 2016; Espinoza et al., 2014). This situation brought an anticyclonic circulation centered around southeastern Brazil, which favored the moisture transport towards the southwestern Amazon. These anomalies occurred during weak La Niña forcing in the Pacific Ocean, but such subtropical-induced anomalous atmospheric mechanisms were associated with tropical ocean variability such as El Niño (Rodrigues et al., 2015).

In addition to the year-to-year variability, a clear multidecadal variability was also documented in this region with dry and wet periods of around 12–14 years (Segura et al., 2016; Sulca et al., 2024). The variability of zonal winds at 200 hPa, associated with the development of the BH, has been proposed as the main mechanism explaining the seasonal and multiannual variability of rainfall in the Altiplano (Garreaud et al., 2003; Garreaud and Aceituno, 2001; Segura et al., 2016, 2019, 2020). Another mechanism that controls the summer rainfall variability in the Altiplano is related to the western Amazon convection, particularly intense since the early 2000s (Segura et al., 2020).

Historically, the area of the southern highlands of Peru is the area most prone to the occurrence of droughts (ANA, 2013). It includes the departments of Puno, Cusco, Tacna, Moquegua, Arequipa and Apurimac with 70% of the population economically active in rainfed agriculture and livestock. The exceptional drought of 1982-83 associated with a very strong El Niño event affected dramatically the entire Altiplano and adjacent Andean valleys (Lovón, 1985) and thus the highlands of Puno and Cusco provinces in Peru and La Paz, Oruro and Potosi provinces in Bolivia. It caused a massive migration from the rural Bolivian Altiplano to the main cities that initiated the explosive population growth of the city of El Alto. It also contributed to the economical downfall associated with the mining crisis in the following years. Between 1981 and 2015, other drought events were milder than the 1982-83 drought and were more localized in the Peruvian Altiplano (Alonso et al., 2022) and Bolivian Altiplano (Canedo-Rosso et al., 2021).

During 2022 and 2023, unprecedented dry conditions were reported in the Peruvian-Bolivian Altiplano in the absence of El Niño conditions (Marengo et al., 2023; Gestión, 2023). Actually, late 2022 – early 2023 was characterized by the end of a three-year-lasting La Niña event (see Figure S1 and Blunden et al., 2023). The level of Lake Titicaca decreased 84 cm between April 2022 and April 2023, with a very weak seasonal lake level increase of only 0.09 m between December 2022 and April 2023. Such low increase revealed very dry conditions not seen since 1982/83 and 1939/40, which were characterized by El Niño conditions (Fig. 1b–d). Outstandingly, the pre-wet season of October–November was the driest in 58 years in several Peruvian Andean cities. Lower than half the normal precipitation in November–December was recorded in some Bolivian cities, the driest since the decade of 1950 (Marengo et al., 2023). This dry condition extended until January 2023 and caused significant water deficits. Such deficit generated heavy economic losses in the regions around the Lake Titicaca. In the provinces of Puno and La Paz, up to 80% of potato and sweet potato and 90% of Andean grains harvests were lost (Guardamino, 2023). The present study aims to describe and analyze the meteorological characteristics and

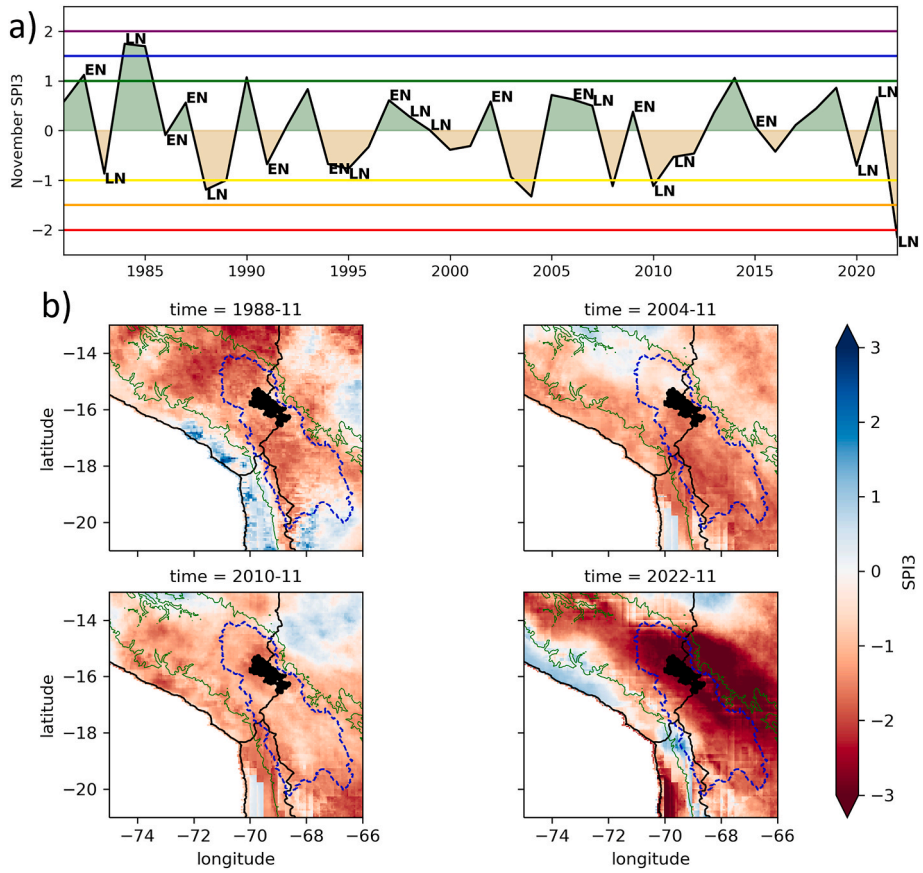

Fig. 3. Interannual rainfall variability over the TDPS system. a) Time-series of mean November SPI3. Colored horizontal lines in −1, −1.5 and −2 (1, 1.5 and 2) represent moderately dry (wet), very dry (wet) and excessively dry (wet) threshold conditions, respectively. Selected El Niño (La Niña) Novembers are tagged with a bold "EN" ("LN") if the El Niño 3.4 index from the ERA5 reanalysis is higher (lower) than 0.75 (−0.75) during that month. b) The four driest Novembers according to a). A blue dashed line delineates the TDPS area, a black polygon bounds the Titicaca Lake area and altitudes of 3 000 m.a.s.l. are bounded by green lines. (For interpretation of the references to color in this figure legend, the reader is referred to the Web version of this article.)

precipitation deficits of the unprecedented 2022-23 drought in the TDPS, particularly during the pre-wet season (September–December).

2. Datasets

2.1. Geomorphological settings

The Shuttle Radar Topographic Mission (SRTM) 30m topography data (https://earthexplorer.usgs.gov/) was used to delimit the Andean regions higher than 3 000 m.a.s.l. in some analyses. The boundaries and area of the TDPS was obtained from the HydroBASINS dataset (https://www.hydrosheds.org/products/hydrobasins), specifically from the Level 05 dataset, according to the Pfaffstetter coding system. The watershed area comprises 145 747 km^2, and its elevation ranges from 3 660 to 6 542 m.a.s.l. (UNEP, 1996), with an average of 4 079 m.a.s.l. The area of the TDPS was obtained from the HydroLAKES dataset (https://www.hydrosheds.org/products/hydrolakes). The lake extends over a surface of 8 269.7 km^2 in average with a mean water level of 3 809.4 m. a.s.l.

2.2. Hydro-climatological datasets

We used monthly water level data collected at Muelle Enafer station (3 800 m.a.s.l.) in the Peruvian side of the Lake Titicaca from 1914 to 2023, provided by the National Meteorology and Hydrology Service (SENAMHI) of Perú (Fig. 1a). We use this timeseries as a reliable indicator of interannual regional rainfall variability over the TDPS, as it is closely correlated with accumulated precipitation during the wet season (Garreaud and Aceituno, 2001; Segura et al., 2016). We define a hydrological year from September of year "n-1" to August of next "n" year. We focus on the October–April period, when the average ascending limb of the Titicaca Lake hydrograph occurs. Estimations of rainfall anomalies during the 1979–2023 period were obtained from Climate Hazards Group InfraRed Precipitation with Station data (CHIRPS version 2.0, (Funk et al., 2015), available at a 0.05° × 0.05° resolution. To assess droughts, the Standardized Precipitation Index, SPI (specifically SPI3) was derived from rainfall anomalies. For standardization purposes, monthly precipitation series was fitted to a Gamma distribution with parameters given by the L-moments method, and then its cumulative probability density function was transformed to a normal distribution through an equiprobability transformation.

2.3. Ocean-atmospheric reanalysis dataset

Oceanic and atmospheric features, including SST, zonal and meridional vertically integrated moisture flux from Earth's surface to the top of the atmosphere (VIMF) and its divergence, and geopotential heights at 200 hPa, were obtained from ERA5 global reanalysis at a monthly timestep (Hersbach et al., 2020). Anomalies were calculated using a 1980–2020 climatology.

To assess the role of the Pacific Ocean SST anomalies, El Niño 3.4 index was obtained after passing a 5-month rolling mean to the 5°N-5°S and 170°W-120°W SST anomalies from the ERA5 dataset. ERA5-based SST anomalies in the southwestern tropical Pacific (15–25°S and 145–195°W) were also calculated. In addition, El Niño 3.4 index derived from the HadiSST dataset (Rayner et al., 2003) was used in order to tag

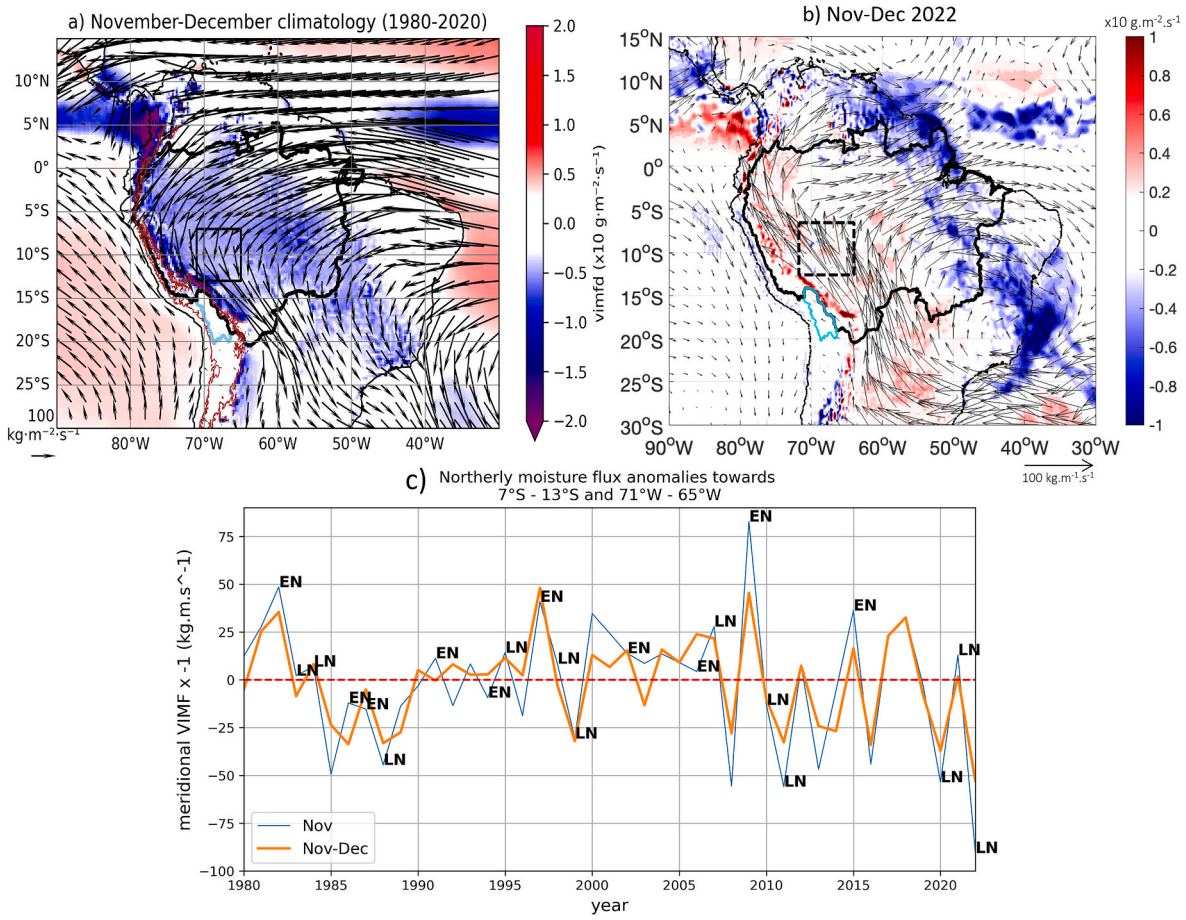

Fig. 4. a) The climatology of November–December 1980–2020 of vertically integrated water vapor flux (VIMF, vectors) and its divergence (shades). b) Anomalies of VIMF and its divergence during November–December 2022. Only anomalies of divergence of VIMF higher (lower) than 2 g $m^{-2}.s^{-1}$ are plotted. Anomalies are computed considering the climatology displayed in a). A black line represents the boundaries of the Amazon basin, the Titicaca Lake basin is bounded by a skyblue line, and heights of 3 000 m.a.s.l. are delineated by brown lines in b). c) Interannual time-series of November, and November–December meridional VIMF anomalies towards 71°-65°W and 13°-7°S (dashed black lines box in a)). Selected El Niño (La Niña) Novembers are tagged with a bold "EN" ("LN") if the El Niño 3.4 index from the ERA5 reanalysis is higher (lower) than 0.75 (−0.75) during that month. (For interpretation of the references to color in this figure legend, the reader is referred to the Web version of this article.)

El Niño and La Niña years since 1914 (i.e., the start year of Muelle Enafer's lake water level measurements).

To identify El Niño (La Niña) events over more than three-month periods (e.g., $December_{(n-1)}$ to $April_{(n)}$ and $December_{(n-1)}$ to $January_{(n)}$). HadISST-derived El Niño 3.4 index must be higher (lower) than 0.75 °C (−0.75 °C) during, at least, 4 months between $April_{(n)}$ and $October_{(n-1)}$. As mentioned before, "n" here denotes the second calendar year of the hydrological year, which starts in September of year "n-1" and finishes in August of year "n". However, when analyzing shorter periods such as single months, ERA5-based El Niño 3.4 index are used for that month instead.

In addition, 200 hPa geopotential height anomalies were computed in southeastern Brazil - 15°S-30°S and 60°W-45°W-, and were used as a proxy for Rossby wave activity over central South America (e.g., Gelbrecht et al., 2018). Extratropical Rossby waves activity can greatly influence the upper and lower tropospheric circulation (e.g., BH's strength and position, and low-level moisture transport), which leads to significant impacts in precipitation over the tropical Andes (e.g., Grimm, 2011; Jones et al., 2023; Sulca et al., 2016, 2018a).

3. The hydro-climatological context for the 2022-23 drought

An unusually low lake level rise (0.09 m) was recorded between December 2022 and April 2023. It represents the fourth lowest seasonal lake rise since 1940 (Fig. 1b). Lower rises were measured only in 1940 and 1983, when lake level difference reversals are found, and in 1990. The years 1940 and 1983 were characterized by, at least, 4 months between October–April under El Niño 3.4 conditions. If the monthly period of lake water level differences is shortened from $April_{(n)}$ – $December_{(n-1)}$ to $February_{(n)}$ – $December_{(n-1)}$ or $January_{(n)}$ – $December_{(n-1)}$ (Fig. 1c–d), the 2022-23 dry anomaly appears stronger when compared to other hydrological years, especially during the 1980–2020 period. This is particularly accentuated between $January_{(n)}$-$December_{(n-1)}$ (Fig. 1d), when even a decrease of lake water levels was registered.

We further employ CHIRPS-derived rainfall anomalies, which is justified by the substantial control (i.e. high, statistically significant correlations) exerted by rainfall on monthly lake level changes during the wet and pre-wet season (Fig. 2). Indeed, seasonal lake water level differences are explained by summertime basin-wide averaged precipitation anomalies over TDPS, accounting for up to 79% of its variance (Fig. 2a). In addition, a significant fraction of the pre-wet lake water level differences can also be explained by pre-wet season rainfall anomalies ($p < 0.05$; Fig. 2b).

Indeed, while the averaged SPI3 over the TDPS shows that the summer of 2023 represented the fourth driest January–March (JFM) quarter (−1.28) since 1981 (Figure S2), 2022 featured the driest September–November (SON) trimester since 1981 (−2.1, Fig. 3a). During the JFM 2023 drought in the TDPS, a severe moisture flux reduction over

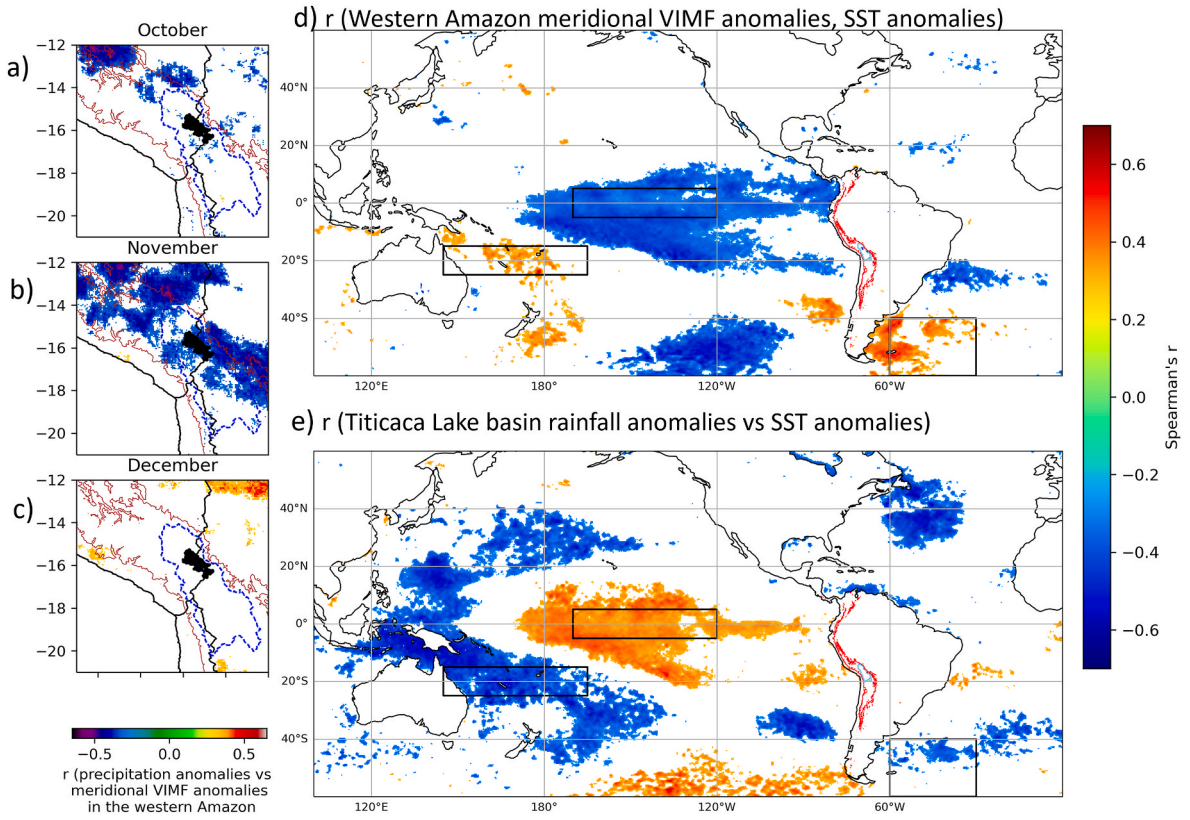

Fig. 5. (a–c) Spearman's correlation coefficient between anomalies of meridional VIMF in 71°-65°W and 13°-7°S (black box in 3a) and precipitation anomalies in the TDPS system during October–November between 1981 and 2022. (d) Spearman's correlation coefficient between anomalies of meridional VIMF in 71°-65°W and 13°-7°S, and SST anomalies during November (1979–2022). (e) Spearman's correlation coefficient between precipitation anomalies in the TDPS system, and SST anomalies during November between 1981 and 2022. Only grid cells where p-value is below 0.05 are shown. Black boxes in d and e bound the areas used to calculate the El Niño 3.4 index, southwestern Pacific SST anomalies and southern subtropical southern Atlantic SST anomalies.

the western Amazon basin was observed, related to the Amazon basin drought in 2023 (Espinoza et al., 2024),. The SPI3 during SON 2022 is equivalent to a diminution in rainfall of 57% if 1981–2020 SON rainfall climatology is considered. The spatial pattern of SPI3 during the four driest SON since 1981 (1988, 2004, 2014 and 2022) shows that, during the 2022 event intense dry conditions were observed in the eastern Andean-Amazon slopes, adjacent to the TDPS (SPI3 < -2) (Fig. 3b). This pattern suggests a potential influence of moisture flux anomalies from Amazonia into the development of dry conditions in the Altiplano.

4. Moisture flux and its large-scale drivers during dry November in the TDPS

According to the 1980–2020 climatology of VIMF and its divergence, moisture flux towards the TDPS is associated with north-to-south moisture flux over the Amazon basin, reaching values of about 100–150 kg $m^{-2}.s^{-1}$ over the western Amazon (Fig. 4a). November–December 2022 was characterized by strong southerly VIMF anomalies and lower-than-normal moisture flux divergence towards the southern and western Amazon basin, which favored subsidence and dry conditions over these regions (Fig. 4b). These features were associated with a low-level cyclonic anomaly centered over southeastern Brazil, where moisture flux convergence was enhanced. An increase of moisture flux convergence was also displayed in Northern South America, centered around 7°N 55°W. If the climatological period of 1980–2020 is considered, meridional VIMF (*-1) anomalies timeseries in the western Amazon (see black box in Fig. 4a) show that the expected north-to-south moisture flux anomaly during November–December 2022 was the weakest since, at least, 1980 (Fig. 4c). November 2022 shows an even stronger north-to-south moisture flux anomaly than other La Niña Novembers.

A significant correlation (~0.5, $p < 0.05$) arises between the timeseries of meridional VIMF in the western Amazon and rainfall timeseries in grid cells of the southern tropical Andes during November and it weakens during the remainder of the pre-wet season between 1981 and 2022 (Fig. 5a–c). Strong interannual variability seen in meridional VIMF variability in the western Amazon in Fig. 4b can be associated with large-scale SST variability, particularly in the Tropical Pacific Ocean (e.g., Jones et al., 2023; Taschetto et al., 2020). If correlated with the timeseries of each grid cell of SST anomalies, it exhibits statistically significant negative correlations with the SST in the central Pacific Ocean during November ($r = 0.4$, $p < 0.05$, Fig. 5d). This means that, during El Niño (La Niña) conditions, there are stronger northerly (southerly) moisture flux anomalies, strengthening (weakening) the moisture advection towards the TDPS and, thus, precipitation processes in this Andean region. This is consistent with previous studies during springtime in the western Amazon basin (De Souza et al., 2021; Espinoza et al., 2011; Jones et al., 2023; Kayano et al., 2021). Furthermore, a spatially-sparse, but significatively correlated positive signal appears in the southwestern tropical Pacific. A similar spatial pattern is obtained when correlating SST anomalies to the TDPS rainfall anomalies during November, when El Niño (La Niña) conditions are correlated with positive (negative) rainfall anomalies ($r = 0.5$, $p < 0.05$, Fig. 5e). The magnitude of the correlation between southwestern Pacific SST and TDPS rainfall anomalies ($r = 0.49$, $p < 0.05$, Fig. 5e) is stronger than the magnitude of the correlation between those SST anomalies and meridional VIMF anomalies in the western Amazon ($r = 0.31$, $p < 0.05$, Fig. 5d). In addition, these variables also feature a subtropical gradient correlation pattern with the SST in the Southern Atlantic Ocean. The southern subtropical southern Atlantic Ocean SST anomalies (40–60°S –

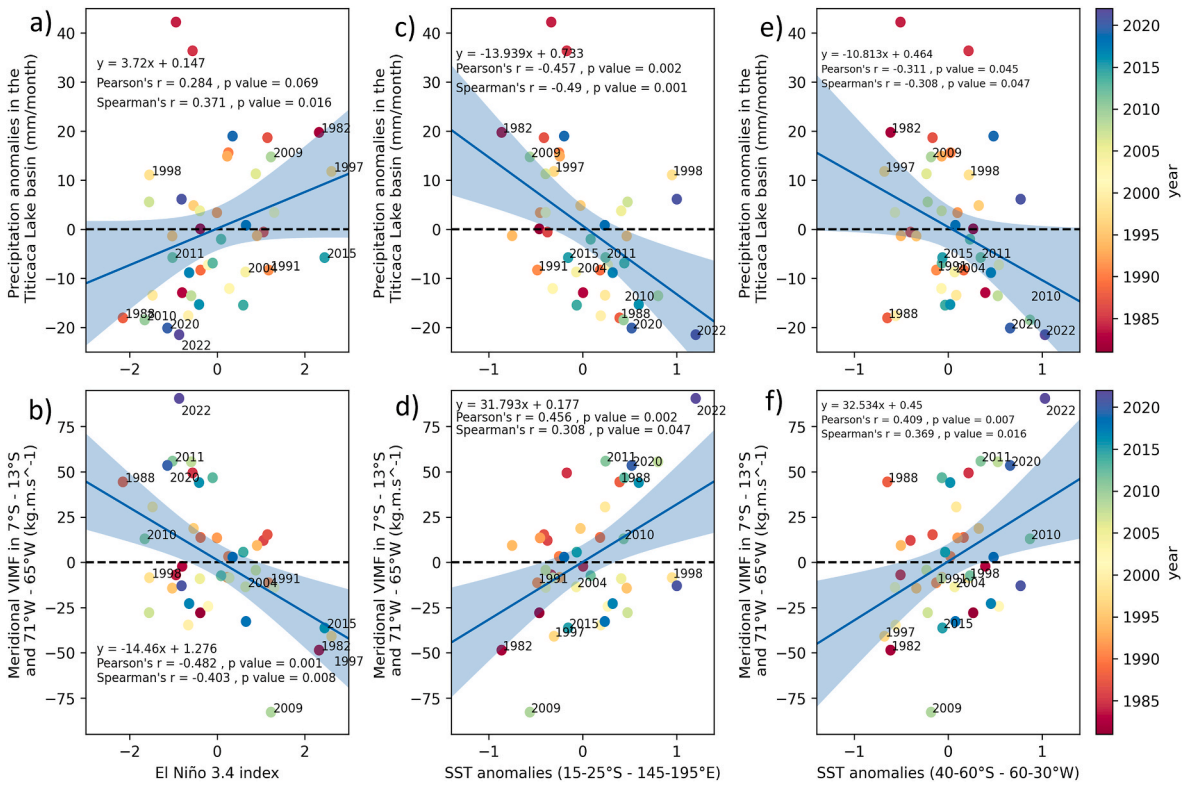

Fig. 6. Central and southwestern tropical Pacific SST relationship with TDPS system rainfall and moisture flux in the western Amazon during November. Scatterplots showing the relationship of El Niño 3.4 index (a–b), southwestern tropical Pacific SST anomalies (c–d), and southern subtropical southern Atlantic SST anomalies (e–f) and precipitation anomalies in the TDPS system(a-c-e), and anomalies of meridional VIMF in 71°-65°W and 13°-7°S (b-d-f). Linear regression lines are delineated by blue solid lines. Blue envelopes around it represents the 95% confidence interval. Regions where the SST anomalies were calculated are bounded in Fig. 5d–e. (For interpretation of the references to color in this figure legend, the reader is referred to the Web version of this article.)

60-30°W, black box in Fig. 5d–e) exhibit statistically significant correlations ($p < 0.05$) of −0.31 with meridional VIMF in the western Amazon and of −0.37 with rainfall anomalies over the TDPS. However, the northern region adjacent to it does not (not shown).

The analysis of the correlations between SST anomalies of the three aforementioned oceanic regions with meridional VIMF in the western Amazon and rainfall over the TDPS are extended by means of scatterplots in Fig. 6. While November El Niño 3.4 index is significatively correlated with the TDPS rainfall anomalies and meridional VIMF in western Amazon, anomalies such as those seen in November 2022 fall well outside the constructed linear regressions (Fig. 6a–b). However, both the November 2022 rainfall and meridional VIMF anomalies appear more as outliers of linear relationships with the southwestern Pacific SST anomalies, November 2022 being the hottest November in that oceanic region since 1981 at least (Fig. 6c–d). This also occurs when considering the SST anomalies over the southern subtropical southern Atlantic Ocean, November 2022 being also the hottest November since at least 1981 (Fig. 6e–f). Thus, a compositional analysis of VIMF and rainfall anomalies for the 5 warmest and coldest Novembers over the three oceanic regions under analysis was carried out, leading to results consistent with this analysis (Figure S2, Table S1). These signals suggest the role of large scale tropical and extratropical atmospheric mechanisms in the diminution of moisture flux over the western Amazon and of rainfall in the TDPS during November 2022 (e.g., Geirinhas et al., 2023).

5. Subtropical dynamics related to droughts in the TDPS

We further explore the subtropical dynamics linked to the occurrence of reductions in moisture flux towards the western Amazon basin and droughts in the TDPS. We do so by exploring the spatiotemporal variability of the geopotential height in 200 hPa (Z200) during November 2022, and its correlation with rainfall anomalies in the TDPS, El Niño 3.4 index and meridional VIMF between November 1979–2022 (Fig. 7). November 2022 exhibited an extratropical Rossby wave train pattern, with an outstanding standardized Z200 negative anomaly in southeastern Brazil, which is a common feature during La Niña's November (Fig. 7a–b). At interannual timescales, a downstream crest (upstream trough) pattern over central South America is positively (negatively) correlated with the TDPS rainfall anomalies during November, as seen with the correlation coefficients between Z200 and the TDPS rainfall of 0.4–0.7 ($p < 0.05$, Fig. 7c). This downstream crest (upstream trough) pattern in the high troposphere can be associated with a stronger (weaker) development of the BH, consistent with wet (dry) conditions in the Titicaca Lake basin (Medina Burga, 2020; Segura et al., 2019). This high tropospheric pattern is also associated with a dipole-like behavior of rainfall anomalies in the core region of the South American monsoon, although during the austral summer period (e.g., Gelbrecht et al., 2018, 2021; Sulca et al., 2018a,b). An upstream trough over central South America is associated with southerly moisture flux anomalies in the southern and central Amazon basin (Fig. 7d), which is favorable to conditions associated with cold-air intrusions towards tropical latitudes in South America (Espinoza et al., 2013). The dynamics of cold-air intrusions are associated with an upstream trough at the high troposphere over central South America, affecting the development of cross-equatorial north-to-south moisture fluxes in the Amazon basin (see Fig. 4a). The influence of Z200 over central South America on meridional moisture fluxes can even reach the northern hemisphere, as seen by the negative correlations around 6°N 55°W (Fig. 7d). The trough pattern at central South America can be further favored by La Niña conditions (Fig. 7e) by the activity of extratropical Rossby waves, as seen by the correlational pattern. Similar results are obtained if Z500 is analyzed instead of Z200 (not shown).

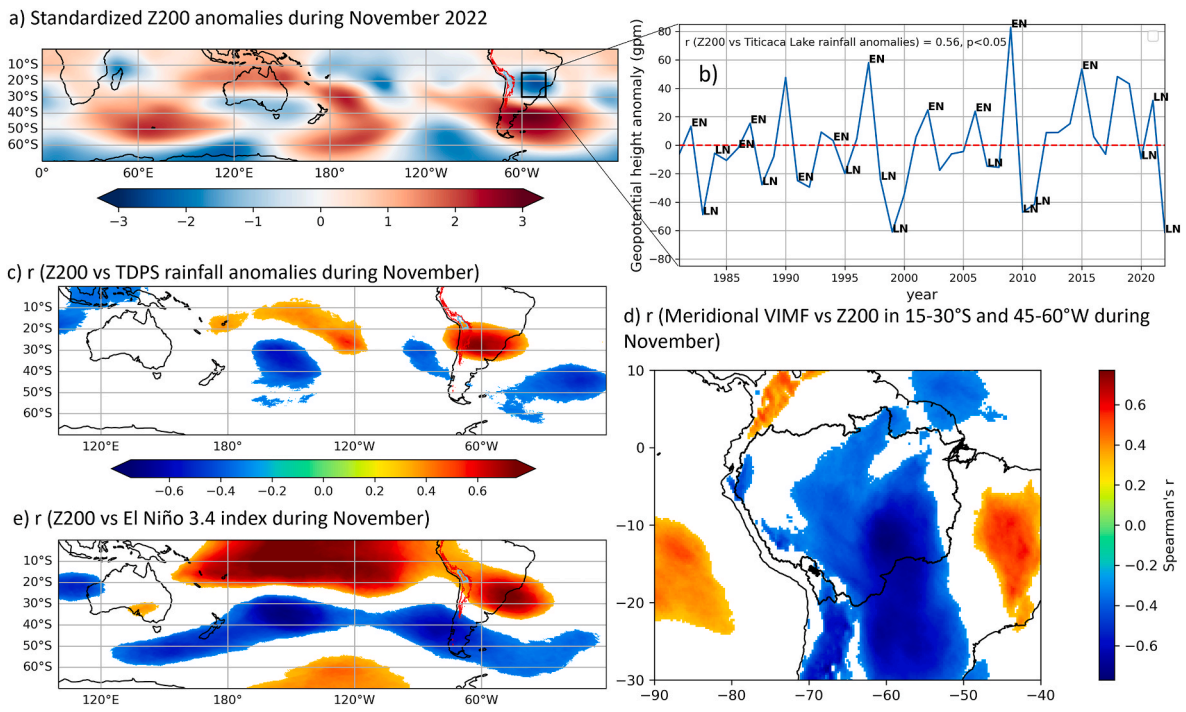

Fig. 7. a) Standardized Z200 anomalies during November 2022, b) Interannual timeseries of Z200 anomalies in 15–30°S and 45–60°W (black box in a)), Spearman correlation coefficients between Z200 and c) TDPS system rainfall anomalies, d) meridional VIMF anomalies in the black box defined in a), and e) El Niño 3.4 index during Novembers. The climatological period considered is 1980–2020. In c-e, Spearman's correlation coefficient values are only shown in grid cells when p-value <0.05. c and d share the same color bar. In b), selected El Niño (La Niña) Novembers are tagged with a bold "EN" ("LN") if the El Niño 3.4 index from the ERA5 reanalysis is higher (lower) than 0.75 (−0.75) during that month. (For interpretation of the references to color in this figure legend, the reader is referred to the Web version of this article.)

Comparisons of composites of 200 hPa winds considering its climatology (1980–2020, Fig. 8a), the 9 wettest (Fig. 8b) and the 9 driest (Fig. 8c) Novembers in the TDPS show a hindered formation of the BH during dry Novembers (Fig. 8c). This weakening is associated with upper-level cyclonic anomalies centered over southeastern South America (Fig. 8d). This feature is associated with the signal over central South America derived from the Z200 – TDPS rainfall correlations, and with the anomalous anticyclone over central-eastern South America derived from the Z200 – El Niño 3.4 index correlations (Fig. 7c–e), which resembles the activity of Rossby wave trains. Regressing atmospheric fields (VIMF and Z200) onto El Niño 3.4 SST index during November for the period 1979–2022, show that La Niña-associated SST anomalies are significantly related to the reduced moisture influx in the western Amazon basin via the influence of extratropical Rossby waves activity, as seen by the slope of the linear regression of Z200 onto El Niño 3.4 index (Fig. 9). This feature subsequently weakens the development of the BH and the north-to-south moisture transport from the Amazon basin (Fig. 9). In addition, a significant relationship between El Niño 3.4 index and VIMF occurs both at the Southern Atlantic Convergence Zone (SACZ) and at the Southern Pacific Convergence Zone (SPCZ). For the latter, increased convection in the SPCZ activity is associated with increased moisture flux towards that region during La Niña. As noted by Geirinhas et al. (2023), this situation can serve as a potential source of extratropical Rossby activity towards South America, leading to increased southerly VIMF anomalies towards tropical South America and, ultimately, the TDPS (Fig. 7d).

6. Discussion and conclusions

In this study, we present empirical evidence that the unprecedented drought in the TDPS during the pre-wet season of 2022 was associated with a reduction in the moisture flux incoming from the Amazon basin. We highlight the impact of extratropical Rossby wave trains over the regional South American circulation during November (1979–2022), when the first significant rains over the TDPS occur. This finding is beyond the traditional view of the main El Niño (La Niña) roles in the configuration of summertime dry (wet) anomalies by high tropospheric teleconnections, where El Niño events, notably the strongest ones, are related to dry conditions (e.g., Garreaud et al., 2003; Segura et al., 2020; Sulca et al., 2018a,b; Jonaitis et al., 2021). The atmospheric features associated with TDPS droughts in the pre-wet season (mainly November) during La Niña events are schematized in Fig. 10a. The activity of extratropical Rossby waves produces an anticyclonic (cyclonic) anomaly over southern Argentina (southeastern Brazil). The Rossby wave activity is primarily caused by perturbations forced at the southwestern Pacific Ocean (Geirinhas et al., 2023), although it can be exacerbated by warm conditions in the southern subtropical Atlantic Ocean (dashed brown polygon). These disturbances enhance extratropical frontal activity and southerly wind anomalies towards tropical South America. In addition, it reduces the northerly atmospheric moisture inflow from the western Amazon (purple big arrow) and the moisture flux towards the TDPS (small pink arrows). Such anomalies produce an inhibition of convection over both the Andes-Amazon transition region and the TDPS (red polygon). It also contributes to the weakening of the development of the Bolivian High ("U200" arrow above the Altiplano), which further reduces convective activity over the TDPS. These dynamics differ from traditional El Niño-related droughts during the wet season (DJF), as shown in Fig. 10b (Cai et al., 2020; Sulca et al., 2018a). El Niño-induced Walker and Hadley cell anomalies accelerate moisture flux towards the La Plata basin (Jones et al., 2023), leading to increased moisture flux divergence in the western Amazon and reduced moisture flux towards the TDPS. In addition with the weakened Bolivian High development, these conditions further reduce convective activity over the TDPS (Sulca et al., 2016), and are further reinforced by extratropical Rossby waves (Mo, 2000).

It is worth to notice that the interannual variability of rainfall

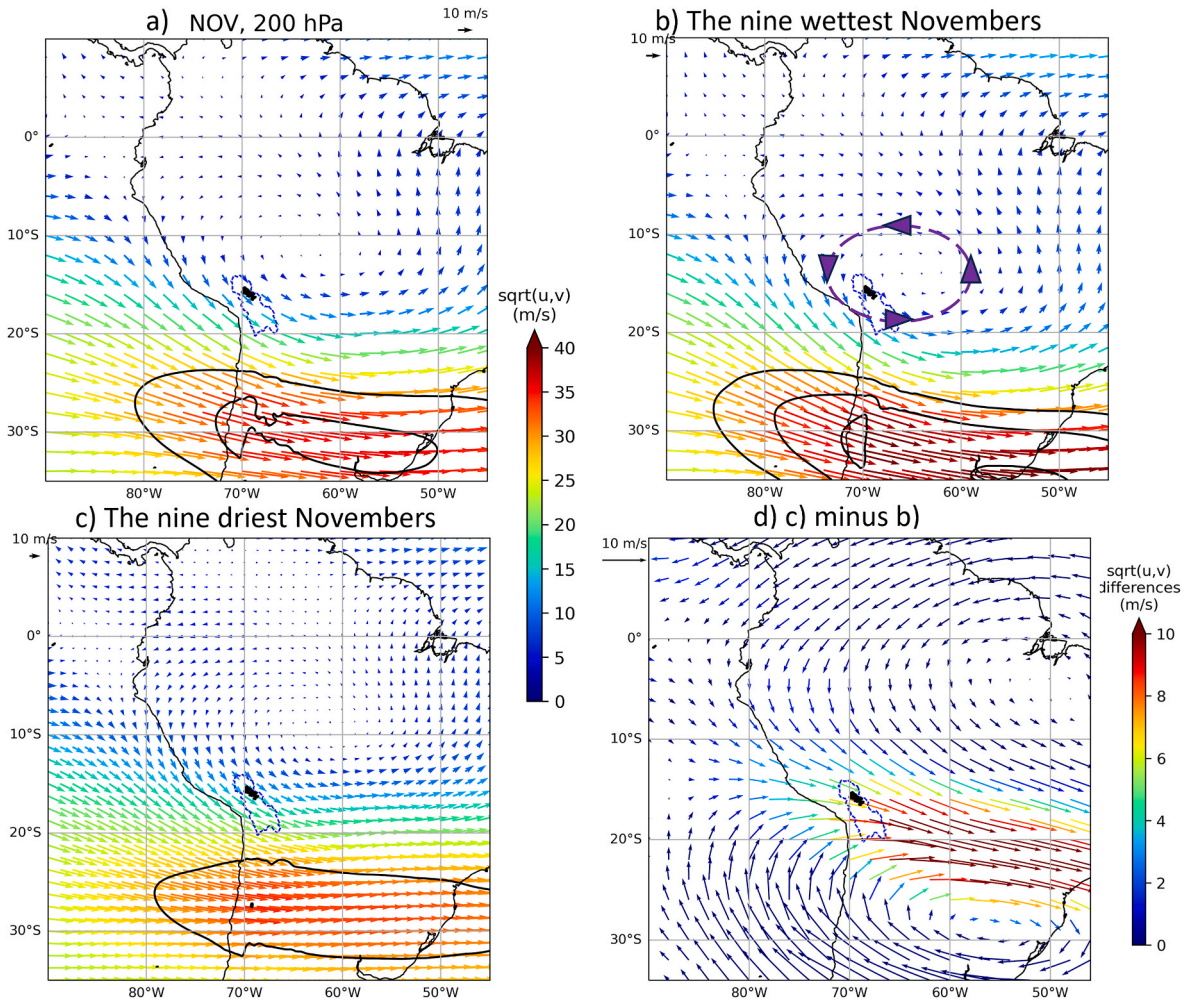

Fig. 8. Upper tropospheric winds (200 hPa) during November. a) The 1980–2020 climatology, b) The nine wettest Novembers in the TDPS system, and c) the nine driest Novembers in the TDPS system. Isotachs of 30, 35 and 40 m/s are drawn in thick black lines, and the TDPS basin is delimited by blue lines. The Titicaca Lake area is bounded by a black polygon. d) The differences between the driest and the wettest Novembers (i.e., c minus b). Note the differences in arrow scales between a-c and d. The period considered in the calculation of wettest and driest Novembers is 1981–2022. In b), an approximated BH circulation is drawn with a dashed ellipse and purple triangles. (For interpretation of the references to color in this figure legend, the reader is referred to the Web version of this article.)

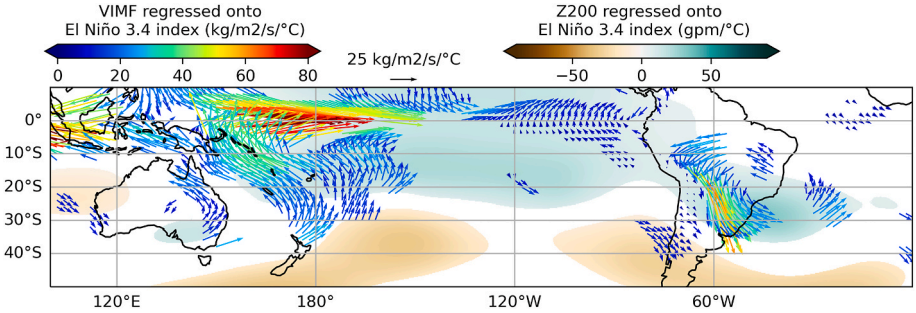

Fig. 9. Regressed atmospheric dynamics fields onto El Niño 3.4 SST index during November (1979–2022). Slope of zonal and meridional regressed VIMF onto El Niño 3.4 index (in vectors and blue-to-red shades), and slope of Z200 regressed onto El Niño 3.4 index (in brown-to-green shades). The pair of zonal and meridional VIMF regression slope vectors are shown if p-value of Pearson's r coefficient between meridional VIMF and El Niño 3.4 index is below 0.05. Similarly, for Z200, regression values are shown only if p-value of Pearson's r coefficient between Z200 and El Niño 3.4 index is below 0.05. (For interpretation of the references to color in this figure legend, the reader is referred to the Web version of this article.)

explained by ENSO in the TDPS is spatially and temporally heterogeneous. During the wet season, ENSO explains a significant fraction of the interannual variability of rainfall in the western side of the TDPS, but less so in its eastern side (Jonaitis et al., 2021). In addition, not all El Niño events are associated with droughts in the TDPS, as not all of them are associated with westerly upper tropospheric winds over the region (Imfeld et al., 2019). Moreover, recently established connection of the southern Andean rainfall variability with the western Amazon convective activity during the summer (Segura et al., 2019) adds more complexity to the picture, suggesting a stronger Andean-Amazon

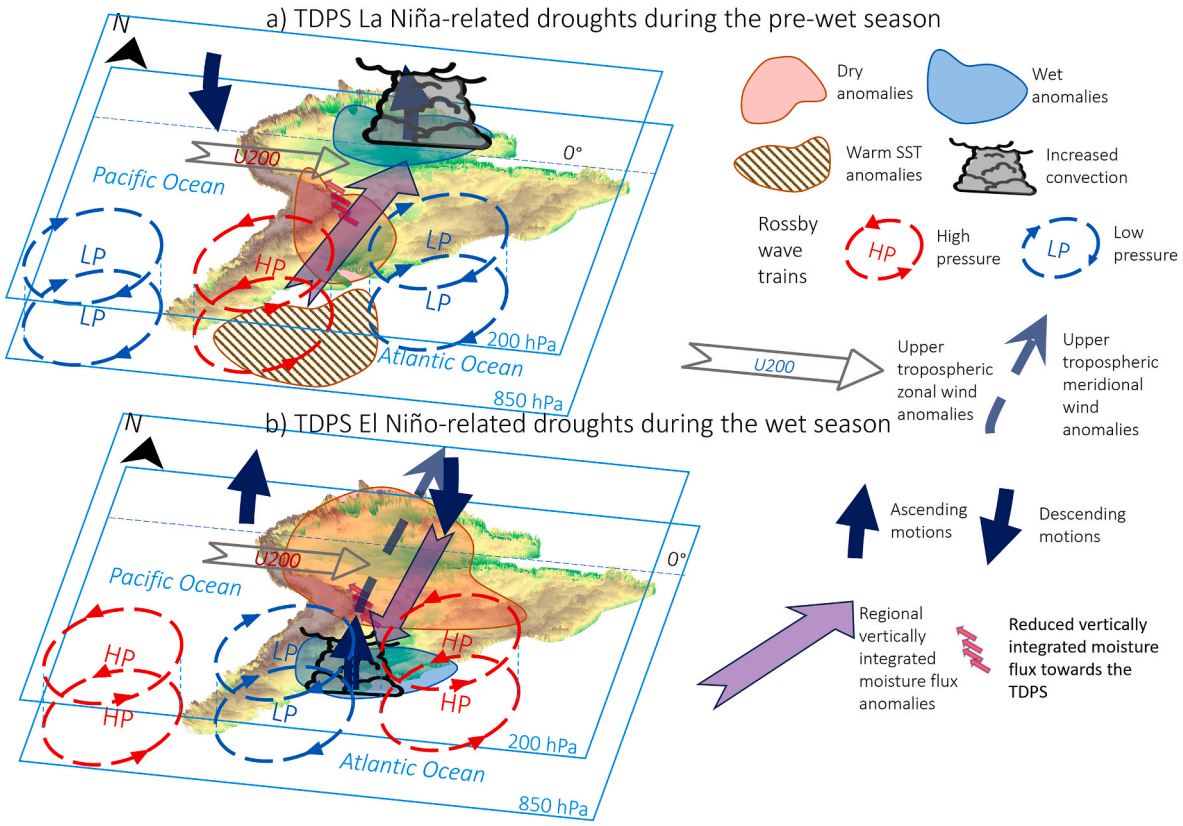

Fig. 10. A simplified conceptual model of the atmospheric mechanisms associated with: a) La Niña-induced droughts in the TDPS during the pre-wet season, and b) El Niño-induced droughts in the TDPS during the wet season. The former resumes the findings of this study, and the latter is a simplified reconstruction based on relevant literature cited in the Introduction.

connection since the early 2000s. The latter helps to explain some characteristics of this extreme drought: i) a stronger rainfall deficit in the eastern part of TDPS (Fig. 3b) and ii) a stronger influence of atmospheric moisture flux from the Amazon on precipitation in the eastern side of the TDPS (Fig. 5b).

It has been suggested that multiyear La Niña conditions, like the recent 3-year La Niña during 2020-22, have stronger impacts than single-year La Niña events on South American and global hydroclimate (Huang et al., 2022; Lopes et al., 2022; Okumura et al., 2017; Raj Deepak et al., 2019; Wang et al., 2023). The longer persistence of multiyear La Niña conditions, while dependent on initial conditions, can induce significant ocean-atmospheric teleconnections in other oceanic basins such as the northern Pacific, the tropical Atlantic and the Indian Oceans, and vice-versa (Hasan et al., 2022; Kim and Yu, 2022; Liao and Wang, 2021; Rodríguez-Fonseca et al., 2009; Tokinaga et al., 2019). Thus, the teleconnections induced by such SST anomalies might interact, leading to the possibility of reinforced atmospheric circulation anomalies for the latter years of multiyear La Niñas. In addition, central Pacific La Niña is also able to exert significant control in the subtropical Atlantic SST variability through Rossby waves activity (Rodrigues et al., 2015). Significant warming was observed in the southern subtropical southern Atlantic Ocean (Fig. 6e and f), which could have aggravated the severity of the drought under study due to reduced moisture flux towards the western Amazon.

Other than 2020-22, only three 3-year La Niña events have occurred since the 1950s: 1954-56, 1973-76 and 1998–2001 (https://earthobservatory.nasa.gov/images/150691/la-nina-times-three). Heterogeneous impacts have been observed in the TDPS during those 3-year La Niña events (Fig. 1b–d). However, the SON strong droughts of the latter years of the 1954-56 and 2020-22 were followed by dry conditions during DJF of the following year. Another similarity between both periods resides on negative January–December lake water level differences (Fig. 1b). For example, Geirinhas et al. (2023) showed that recent drought events (2019–2022) in central-eastern South America were associated to a significant weakening of northerly moisture flux towards that region, an anomaly seen in the present study. In addition, significant negative moisture flux anomalies in that region were also present by the end of the decade of 1950, both being associated with cold SST anomalies in the central Tropical Pacific Ocean. However, the reduction in moisture transport in the western Amazon during November 2022 has not been seen, at least, since the 1950s (Figure S4). In addition, a hypothesized mechanism suggests that strong El Niño events preceded triple-dip La Niña events; and while this was the case for the 1998–2001 event, it was not for the 1954-56 and 2020-22 events (Kim et al., 2023; Shi et al., 2023). For the 2022-23 La Niña event, intertropical and extratropical interactions were suggested to trigger and sustain that La Niña event (e.g., Hasan et al., 2022; Shi et al., 2023), although the synergistic impacts on the causes and the consequences of that event still need further investigation.

While the atmospheric features addressed in the present study (i.e., extratropical Rossby waves, moisture flux anomalies from Amazonia) are related to SST variability and La Niña 2022-23, the fact that in November 2022 exceptional dry conditions were observed cannot be fully explained by the Pacific Ocean SST variability. Other mechanisms must be analyzed, for instance the modulation of shorter frequency variability modes, such as the Madden Julian Oscillation (Fernandes and Grimm, 2023; Jones et al., 2023), the potential impact of global warming and Amazonian deforestation. Regarding global warming, It is still worth to explore future projections over complex terrain such as the Andes-Amazon transition region (e.g., Gutierrez et al., 2024). Future climate projections studies suggested significant reductions in precipitation and increases in the intensity, frequency and duration of droughts

over the TDPS (Minvielle and Garreaud, 2011; Zubieta et al., 2021). Although the origins of October–December 2022 drought in subtropical South America were contained within the thresholds of natural variability, human activity significatively amplified the consequences of that compound hot and dry event (Arias et al., 2023). Finally, the potential role of deforestation rates in Amazonia in this drought cannot be ruled out. Studies of projected Amazon deforestation scenarios showed that it is associated with reductions in evapotranspiration, water vapor and moisture fluxes, and lengthening of the dry season; all of which inhibit convective activity in the western Amazon and, ultimately, precipitation over the tropical Andes (Commar et al., 2023; Ruiz-Vásquez et al., 2020; Sierra et al., 2022, 2023; Wongchuig et al., 2023), Such atmospheric features agree with those characterizing the 2022 drought in the Altiplano, but the role of ongoing deforestation in the causes and consequences of this specific drought have not been addressed yet. Therefore, we encourage further research about global warming and Amazon deforestation impacts over the southern Tropical Andes and the Altiplano region.

CRediT authorship contribution statement

Ricardo A. Gutierrez-Villarreal: Writing – review & editing, Writing – original draft, Visualization, Validation, Supervision, Software, Resources, Project administration, Methodology, Investigation, Funding acquisition, Formal analysis, Data curation, Conceptualization. **Jhan-Carlo Espinoza:** Writing – review & editing, Writing – original draft, Visualization, Validation, Supervision, Resources, Project administration, Methodology, Investigation, Funding acquisition, Formal analysis, Conceptualization. **Waldo Lavado-Casimiro:** Writing – review & editing, Resources, Conceptualization. **Clémentine Junquas:** Writing – review & editing, Visualization, Validation, Supervision, Methodology, Formal analysis. **Jorge Molina-Carpio:** Writing – review & editing, Writing – original draft, Visualization, Validation, Conceptualization. **Thomas Condom:** Writing – review & editing, Writing – original draft, Visualization, Validation, Methodology, Conceptualization. **José A. Marengo:** Writing – review & editing, Writing – original draft, Visualization, Validation, Conceptualization.

Declaration of competing interest

The authors declare that they have no known competing financial interests or personal relationships that could have appeared to influence the work reported in this paper.

Data availability

Data will be made available on request.

Acknowledgements

This work has been funded by the Water Cycle and Climate Change project (CECC; IRD/AFD) and by the International Research Network (IRN) ANDES C2H of the IRD. JAM was supported by Brazil's National Institute of Science and Technology for Climate Change Phase 2 under CNPq Grant 465501/2014-1; FAPESP Grants 2014/50848-9, and the National Coordination for Higher Education and Training (CAPES) Grant 88887.136402/2017-00. JMC was supported by the Universidad Mayor de San Andrés (UMSA) within the framework provided by the Laboratoire Mixte International (LMI) Altiplano.

Appendix A. Supplementary data

Supplementary data to this article can be found online at https://doi.org/10.1016/j.wace.2024.100710.

References

Alonso, W.A., Lavado-Casimiro, W., Espinoza-Villar, R., Chávarri-Velarde, E., 2022. Spatial distribution of droughts in the Titicaca Lake basin. Revista Brasileira de Meteorologia 37, 289–304. https://doi.org/10.1590/0102-77863730054.

ANA, 2013. Las Condiciones de Sequía y Estrategias de Gestión en el Perú. In: Informe Nacional del Perú. Autoridad Nacional del Agua, Lima, p. 11.

Arias, P.A., Garreaud, R., Poveda, G., Espinoza, J.C., Molina-Carpio, J., Masiokas, M., Viale, M., Scaff, L., van Oevelen, P.J., 2021. Hydroclimate of the Andes Part II: hydroclimate variability and sub-continental patterns. Front. Earth Sci. 666.

Arias, P.A., Rivera, J.A., Sörensson, A.A., Zachariah, M., Barnes, C., Philip, S., Kew, S., Vautard, R., Koren, G., Pinto, I., Vahlberg, M., Singh, R., Raju, E., Li, S., Yang, W., Vecchi, G.A., Otto, F.E.L., 2023. Interplay between climate change and climate variability: the 2022 drought in Central South America. Climatic Change 177 (1), 6. https://doi.org/10.1007/s10584-023-03664-4.

Blunden, J., Boyer, T., Bartow-Gillies, E., 2023. State of the climate in 2022. Bull. Am. Meteorol. Soc. 104 (9), S1–S516. https://doi.org/10.1175/2023BAMSStateoftheClimate.1.

Cai, W., McPhaden, M.J., Grimm, A.M., Rodrigues, R.R., Taschetto, A.S., Garreaud, R.D., Dewitte, B., Poveda, G., Ham, Y.-G., Santoso, A., Ng, B., Anderson, W., Wang, G., Geng, T., Jo, H.-S., Marengo, J.A., Alves, L.M., Osman, M., Li, S., et al., 2020. Climate impacts of the el niño–southern oscillation on SouthSouth America. Nat. Rev. Earth Environ. 1 (4) https://doi.org/10.1038/s43017-020-0040-3. Article 4.

Canedo-Rosso, C., Hochrainer-Stigler, S., Pflug, G., Condori, B., Berndtsson, R., 2021. Drought impact in the Bolivian Altiplano agriculture associated with the El Niño–Southern Oscillation using satellite imagery data. Nat. Hazards Earth Syst. Sci. 21 (3), 995–1010. https://doi.org/10.5194/nhess-21-995-2021.

Coelho, C.A.S., de Oliveira, C.P., Ambrizzi, T., Reboita, M.S., Carpenedo, C.B., Campos, J. L.P.S., Tomaziello, A.C.N., Pampuch, L.A., Custódio, M. de S., Dutra, L.M.M., Da Rocha, R.P., Rehbein, A., 2016. The 2014 southeast Brazil austral summer drought: regional scale mechanisms and teleconnections. Clim. Dynam. 46 (11), 3737–3752. https://doi.org/10.1007/s00382-015-2800-1.

Commar, L.F.S., Abrahão, G.M., Costa, M.H., 2023. A possible deforestation-induced synoptic-scale circulation that delays the rainy season onset in Amazonia. Environ. Res. Lett. 18 (4), 044041 https://doi.org/10.1088/1748-9326/acc95f.

De Souza, I.P., Andreoli, R.V., Kayano, M.T., Vargas, F.F., Cerón, W.L., Martins, J.A., Freitas, E., De Souza, R.A.F., 2021. Seasonal precipitation variability modes over South America associated to El Niño-Southern Oscillation (ENSO) and non-ENSO components during the 1951–2016 period. Int. J. Climatol. 41 (8), 4321–4338. https://doi.org/10.1002/joc.7075.

Espinoza, J.C., Garreaud, R., Poveda, G., Arias, P.A., Molina-Carpio, J., Masiokas, M., Viale, M., Scaff, L., 2020. Hydroclimate of the Andes Part I: main climatic features. Front. Earth Sci. 8, 64. https://doi.org/10.3389/feart.2020.00064.

Espinoza, J.C., Marengo, J.A., Ronchail, J., Carpio, J.M., Flores, L.N., Guyot, J.L., 2014. The extreme 2014 flood in south-western Amazon basin: the role of tropical-subtropical South Atlantic SST gradient. Environ. Res. Lett. 9 (12), 124007 https://doi.org/10.1088/1748-9326/9/12/124007.

Espinoza, J.C., Ronchail, J., Guyot, J.L., Junquas, C., Vauchel, P., Lavado, W., Drapeau, G., Pombosa, R., 2011. Climate variability and extreme drought in the upper Solimões River (western Amazon Basin): understanding the exceptional 2010 drought. Geophys. Res. Lett. 38 (13) https://doi.org/10.1029/2011GL047862.

Espinoza, J.C., Ronchail, J., Lengaigne, M., Quispe, N., Silva, Y., Bettolli, M.L., Avalos, G., Llacza, A., 2013. Revisiting wintertime cold air intrusions at the east of the Andes: propagating features from subtropical Argentina to Peruvian Amazon and relationship with large-scale circulation patterns. Clim. Dynam. 41 (7), 1983–2002. https://doi.org/10.1007/s00382-012-1639-y.

Espinoza, J.-C., Jimenez, J.C., Marengo, J.A., Schongart, J., Ronchail, J., Lavado-Casimiro, W., Ribeiro, J.V.M., 2024. The new record of drought and warmth in the Amazon in 2023 related to regional and global climatic features. Sci. Rep. 14 (1), 8107. https://doi.org/10.1038/s41598-024-58782-5.

Espinoza, J.-C., Marengo, J.A., Schongart, J., Jimenez, J.C., 2022. The new historical flood of 2021 in the Amazon River compared to major floods of the 21st century: atmospheric features in the context of the intensification of floods. Weather Clim. Extrem. 35, 100406 https://doi.org/10.1016/j.wace.2021.100406.

Fernandes, L.G., Grimm, A.M., 2023. ENSO modulation of global MJO and its impacts on SouthSouth America. J. Clim. 36 (22), 7715–7738. https://doi.org/10.1175/JCLI-D-22-0781.1.

Funk, C., Peterson, P., Landsfeld, M., Pedreros, D., Verdin, J., Shukla, S., Husak, G., Rowland, J., Harrison, L., Hoell, A., Michaelsen, J., 2015. The climate hazards infrared precipitation with stations—a new environmental record for monitoring extremes. Sci. Data 2 (1), 150066. https://doi.org/10.1038/sdata.2015.66.

Garcia, M., Alavi, G., 2018. Bolivia. In: Núñez Cobo, J., Verbist, K. (Eds.), Atlas de Sequía de América Latina y el Caribe. UNESCO y CAZALAC, La Serena, Chile, pp. 29–42 (in Spanish).

Garcia, M., Raes, D., Jacobsen, S.-E., Michel, T., 2007. Agroclimatic constraints for rainfed agriculture in the Bolivian Altiplano. J. Arid Environ. 71 (1), 109–121. https://doi.org/10.1016/j.jaridenv.2007.02.005.

Garreaud, R., Aceituno, P., 2001. Interannual rainfall variability over the SouthSouth American altiplano. J. Clim. 14 (12), 2779–2789. https://doi.org/10.1175/1520-0442(2001)014<2779:IRVOTS>2.0.CO.

Garreaud, R.D., 2009. The Andes climate and weather. Adv. Geosci. 22, 3–11. https://doi.org/10.5194/adgeo-22-3-2009.

Garreaud, R., Vuille, M., Clement, A.C., 2003. The climate of the Altiplano: observed current conditions and mechanisms of past changes. Palaeogeogr. Palaeoclimatol. Palaeoecol. 194 (1), 5–22. https://doi.org/10.1016/S0031-0182(03)00269-4.

Geerts, S., Raes, D., Garcia, M., Del Castillo, C., Buytaert, W., 2006. Agro-climatic suitability mapping for crop production in the Bolivian Altiplano: a case study for quinoa. Agric. For. Meteorol. 139 (3), 399–412. https://doi.org/10.1016/j.agrformet.2006.08.018.

Geirinhas, J.L., Russo, A.C., Libonati, R., Miralles, D.G., Ramos, A.M., Gimeno, L., Trigo, R.M., 2023. Combined large-scale tropical and subtropical forcing on the severe 2019–2022 drought in South America. Npj Climate and Atmospheric Science 6 (1), 185. https://doi.org/10.1038/s41612-023-00510-3.

Gelbrecht, M., Boers, N., Kurths, J., 2018. Phase coherence between precipitation in South America and Rossby waves. Sci. Adv. 4 (12), eaau3191 https://doi.org/10.1126/sciadv.aau3191.

Gelbrecht, M., Boers, N., Kurths, J., 2021. Variability of the low-level circulation of the South American Monsoon analysed with complex networks. Eur. Phys. J. Spec. Top. 230 (14), 3101–3120. https://doi.org/10.1140/epjs/s11734-021-00187-w.

Gestión, 2023. Senamhi | Nivel de agua del lago Titicaca es el más bajo desde 1999 | lluvias en Perú | PERU. Gestion. https://gestion.pe/peru/senamhi-nivel-de-agua-del-lago-titicaca-es-el-mas-bajo-desde-1999-lluvias-en-peru-noticia/.

Grimm, A.M., 2011. Interannual climate variability in South America: impacts on seasonal precipitation, extreme events, and possible effects of climate change. Stoch. Environ. Res. Risk Assess. 25 (4), 537–554. https://doi.org/10.1007/s00477-010-0420-1.

Guardamino, B., 2023. Puno: continuo descenso del lago Titicaca y sequia del 84% de totorales causan preocupación en la región. Info. https://www.infobae.com/peru/2023/09/26/puno-continuo-descenso-del-lago-titicaca-y-sequia-del-84-de-totorales-causan-preocupacion-en-la-region/.

Gutierrez, R.A., Junquas, C., Armijos, E., Sörensson, A.A., Espinoza, J.-C., 2024. Performance of regional climate model precipitation simulations over the terrain-complex andes-amazon transition region. J. Geophys. Res. Atmos. 129 (1), e2023JD038618 https://doi.org/10.1029/2023JD038618.

Hasan, N.A., Chikamoto, Y., McPhaden, M.J., 2022. The influence of tropical basin interactions on the 2020–2022 double-dip La Niña. Frontiers in Climate 4. https://www.frontiersin.org/articles/10.3389/fclim.2022.1001174.

Hersbach, H., Bell, B., Berrisford, P., Hirahara, S., Horányi, A., Muñoz-Sabater, J., Nicolas, J., Peubey, C., Radu, R., Schepers, D., Simmons, A., Soci, C., Abdalla, S., Abellan, X., Balsamo, G., Bechtold, P., Biavati, G., Bidlot, J., Bonavita, M., et al., 2020. The ERA5 global reanalysis. Q. J. R. Meteorol. Soc. 146 (730), 1999–2049. https://doi.org/10.1002/qj.3803.

Huang, G., Wang, R., Liu, J., Gao, L., Liu, M., Chen, Q., 2022. Seasonally evolving impacts of multiyear La Niña on precipitation in southern China. Front. Earth Sci. 10. https://www.frontiersin.org/articles/10.3389/feart.2022.884604.

Imfeld, N., Barreto Schuler, C., Correa Marrou, K.M., Jacques-Coper, M., Sedlmeier, K., Gubler, S., Huerta, A., Brönnimann, S., 2019. Summertime precipitation deficits in the southern Peruvian highlands since 1964. Int. J. Climatol. 39 (11), 4497–4513. https://doi.org/10.1002/joc.6087.

Jonaitis, J.A., Perry, L.B., Soulé, P.T., Thaxton, C., Andrade-Flores, M.F., Vargas, T.I., Ticona, L., 2021. Spatiotemporal patterns of ENSO-precipitation relationships in the tropical Andes of southern Peru and Bolivia. Int. J. Climatol. 41 (8), 4061–4076.

Jones, C., Mu, Y., Carvalho, L.M.V., Ding, Q., 2023. The South America low-level Jet: form, variability and large-scale forcings. Npj Climate and Atmospheric Science 6 (1), 175. https://doi.org/10.1038/s41612-023-00501-4.

Karoly, D.J., 1989. Southern hemisphere circulation features associated with el niño-southern oscillation events. J. Clim. 2 (11), 1239–1252. https://doi.org/10.1175/1520-0442(1989)002<1239:SHCFAW>2.0.CO.

Kayano, M.T., Cerón, W.L., Andreoli, R.V., Souza, R.A.F., Souza, I.P., Canchala, T., 2021. El niño-southern oscillation and Indian ocean dipole modes: their effects on SouthSouth American rainfall during austral spring. Atmosphere 12 (11), 11. https://doi.org/10.3390/atmos12111437.

Kim, J.-W., Yu, J.-Y., 2022. Single- and multi-year ENSO events controlled by pantropical climate interactions. Npj Climate and Atmospheric Science 5 (1). https://doi.org/10.1038/s41612-022-00305-y. Article 1.

Kim, J.-W., Yu, J.-Y., Tian, B., 2023. Overemphasized role of preceding strong El Niño in generating multi-year La Niña events. Nat. Commun. 14 (1), 6790. https://doi.org/10.1038/s41467-023-42373-5.

Lavado-Casimiro, W., Espinoza, J.C., 2014. Impactos de El Niño y La Niña en las lluvias del Perú (1965-2007). Revista Brasileira de Meteorologia 29, 171–182. https://doi.org/10.1590/S0102-77862014000200003.

Lavado-Casimiro, W.S., Felipe, O., Silvestre, E., Bourrel, L., 2013. ENSO impact on hydrology in Peru. Adv. Geosci. 33, 33–39. https://doi.org/10.5194/adgeo-33-33-2013.

Liao, H., Wang, C., 2021. Sea surface temperature anomalies in the western Indian ocean as a trigger for atlantic Niño events. Geophys. Res. Lett. 48 (8), e2021GL092489 https://doi.org/10.1029/2021GL092489.

Lopes, A.B., Andreoli, R.V., Souza, R.A.F., Cerón, W.L., Kayano, M.T., Canchala, T., de Moraes, D.S., 2022. Multiyear La Niña effects on the precipitation in SouthSouth America. Int. J. Climatol. 42 (16), 9567–9582. https://doi.org/10.1002/joc.7847.

Lovón, G., 1985. El Sur Andino Peruano y la Coyuntura de Sequía: 1982-1983 Buenos Aires. Grupo Editor Latinoamericano, p. 17.

Marengo, J.A., Espinoza, J.C., 2016. Extreme seasonal droughts and floods in Amazonia: causes, trends and impacts. Int. J. Climatol. 36 (3), 1033–1050. https://doi.org/10.1002/joc.4420.

Marengo, J.A., Espinoza, J.C., Alves, L.M., Ronchail, J., Cunha, A.P., Ramos, A.M., et al., 2023. Southern South America [in "state of the climate in 2022". Bull. Am. Meteorol. Soc. 104 (9), S393–S396. https://doi.org/10.1175/2023BAMSStateoftheClimate_Chapter7.1.

Marengo, J.A., Liebmann, B., Grimm, A.M., Misra, V., Silva Dias, P.L., Cavalcanti, I.F.A., Carvalho, L.M.V., Berbery, E.H., Ambrizzi, T., Vera, C.S., Saulo, A.C., Nogues-Paegle, J., Zipser, E., Seth, A., Alves, L.M., 2012. Recent developments on the South American monsoon system. Int. J. Climatol. 32 (1), 1–21. https://doi.org/10.1002/joc.2254.

Medina Burga, M. de J., 2020. Determinación de patrones de vientos horizontales en la tropósfera y su relación con la precipitación en el altiplano peruano boliviano [Universidad Nacional Agraria La Molina]. http://repositorio.lamolina.edu.pe/handle/20.500.12996/4347.

Minvielle, M., Garreaud, R.D., 2011. Projecting rainfall changes over the SouthSouth American altiplano. J. Clim. 24 (17), 4577–4583. https://doi.org/10.1175/JCLI-D-11-00051.1.

Mo, K.C., 2000. Relationships between low-frequency variability in the southern hemisphere and Sea Surface temperature anomalies. J. Clim. 13 (20), 3599–3610. https://doi.org/10.1175/1520-0442(2000)013<3599:RBLFVI>2.0.CO.

Montini, T.L., Jones, C., Carvalho, L.M.V., 2019. The South American low-level Jet: a new climatology, variability, and changes. J. Geophys. Res. Atmos. 124 (3), 1200–1218. https://doi.org/10.1029/2018JD029634.

Okumura, Y.M., DiNezio, P., Deser, C., 2017. Evolving impacts of multiyear La Niña events on atmospheric circulation and U.S. Drought. Geophys. Res. Lett. 44 (22), 11614–11623. https://doi.org/10.1002/2017GL075034.

Poveda, G., Espinoza, J.C., Zuluaga, M.D., Solman, S.A., Garreaud, R., Van Oevelen, P.J., 2020. High impact weather events in the Andes. Front. Earth Sci. 8, 162. https://doi.org/10.3389/feart.2020.00162.

Raj Deepak, S.N., Chowdary, J.S., Dandi, A.R., Srinivas, G., Parekh, A., Gnanaseelan, C., Yadav, R.K., 2019. Impact of multiyear La Niña events on the South and East Asian summer monsoon rainfall in observations and CMIP5 models. Clim. Dynam. 52 (11), 6989–7011. https://doi.org/10.1007/s00382-018-4561-0.

Rayner, N.A., Parker, D.E., Horton, E.B., Folland, C.K., Alexander, L.V., Rowell, D.P., Kent, E.C., Kaplan, A., 2003. Global analyses of sea surface temperature, sea ice, and night marine air temperature since the late nineteenth century. J. Geophys. Res. Atmos. 108 (D14) https://doi.org/10.1029/2002JD002670.

Rodrigues, R.R., Campos, E.J.D., Haarsma, R., 2015. The impact of ENSO on the South Atlantic subtropical dipole mode. J. Clim. 28 (7), 2691–2705. https://doi.org/10.1175/JCLI-D-14-00483.1.

Rodríguez-Fonseca, B., Polo, I., García-Serrano, J., Losada, T., Mohino, E., Mechoso, C.R., Kucharski, F., 2009. Are Atlantic Niños enhancing Pacific ENSO events in recent decades? Geophys. Res. Lett. 36 (20) https://doi.org/10.1029/2009GL040048.

Ruiz-Vásquez, M., Arias, P.A., Martínez, J.A., Espinoza, J.C., 2020. Effects of Amazon basin deforestation on regional atmospheric circulation and water vapor transport towards tropical South America. Clim. Dynam. 54 (9), 4169–4189. https://doi.org/10.1007/s00382-020-05223-4.

Satgé, F., Hussain, Y., Xavier, A., Zolá, R.P., Salles, L., Timouk, F., Seyler, F., Garnier, J., Frappart, F., Bonnet, M.-P., 2019. Unraveling the impacts of droughts and agricultural intensification on the Altiplano water resources. Agric. For. Meteorol. 279, 107710 https://doi.org/10.1016/j.agrformet.2019.107710.

Sedlmeier, K., Imfeld, N., Gubler, S., Spirig, C., Caiña, K.Q., Escajadillo, Y., Rohrer, M., Schwierz, C., 2023. The rainy season in the Southern Peruvian Andes: a climatological analysis based on the new Climandes index. Int. J. Climatol. 43 (6), 3005–3022. https://doi.org/10.1002/joc.8013.

Segura, H., Espinoza, J.C., Junquas, C., Lebel, T., Vuille, M., Condom, T., 2022. Extreme austral winter precipitation events over the South-American Altiplano: regional atmospheric features. Clim. Dynam. 1–18.

Segura, H., Espinoza, J.C., Junquas, C., Lebel, T., Vuille, M., Garreaud, R., 2020. Recent changes in the precipitation-driving processes over the southern tropical Andes/western Amazon. Clim. Dynam. 54 (5–6), 2613–2631. https://doi.org/10.1007/s00382-020-05132-6.

Segura, H., Espinoza, J.C., Junquas, C., Takahashi, K., 2016. Evidencing decadal and interdecadal hydroclimatic variability over the Central Andes. Environ. Res. Lett. 11 (9), 094016 https://doi.org/10.1088/1748-9326/11/9/094016.

Segura, H., Junquas, C., Espinoza, J.C., Vuille, M., Jauregui, Y.R., Rabatel, A., Condom, T., Lebel, T., 2019. New insights into the rainfall variability in the tropical Andes on seasonal and interannual time scales. Clim. Dynam. 53 (1), 405–426. https://doi.org/10.1007/s00382-018-4590-8.

Shi, L., Ding, R., Hu, S., Li, X., Li, J., 2023. Extratropical impacts on the 2020–2023 triple-dip La Niña event. Atmos. Res. 294, 106937 https://doi.org/10.1016/j.atmosres.2023.106937.

Sierra, J.P., Espinoza, J.-C., Junquas, C., Wongchuig, S., Polcher, J., Moron, V., Fita, L., Arias, P.A., Schrapffer, A., Pennel, R., 2023. Impacts of land-surface heterogeneities and Amazonian deforestation on the wet season onset in southern Amazon. Clim. Dynam. 61 (9), 4867–4898. https://doi.org/10.1007/s00382-023-06835-2.

Sierra, J.P., Junquas, C., Espinoza, J.C., Segura, H., Condom, T., Andrade, M., Molina-Carpio, J., Ticona, L., Mardoñez, V., Blacutt, L., 2022. Deforestation impacts on Amazon-Andes hydroclimatic connectivity. Clim. Dynam. 58 (9), 2609–2636.

Sietz, D., Mamani Choque, S.E., Lüdeke, M.K.B., 2012. Typical patterns of smallholder vulnerability to weather extremes with regard to food security in the Peruvian Altiplano. Reg. Environ. Change 12 (3), 489–505. https://doi.org/10.1007/s10113-011-0246-5.

Sulca, J., Apaéstegui, J., Tacza, J., 2024. New insights into the biennial-to-multidecadal variability of the water level fluctuation in Lake Titicaca in the 20th century. Frontiers in Climate 5. https://www.frontiersin.org/articles/10.3389/fclim.2023.1325224.

Sulca, J., Takahashi, K., Espinoza, J.-C., Vuille, M., Lavado-Casimiro, W., 2018a. Impacts of different ENSO flavors and tropical Pacific convection variability (ITCZ, SPCZ) on austral summer rainfall in South America, with a focus on Peru. Int. J. Climatol. 38 (1), 420–435. https://doi.org/10.1002/joc.5185.

Sulca, J., Vuille, M., Roundy, P., Takahashi, K., Espinoza, J.-C., Silva, Y., Trasmonte, G., Zubieta, R., 2018b. Climatology of extreme cold events in the central Peruvian Andes

during austral summer: origin, types and teleconnections. Q. J. R. Meteorol. Soc. 144 (717), 2693–2714. https://doi.org/10.1002/qj.3398.

Sulca, J., Vuille, M., Silva, Y., Takahashi, K., 2016. Teleconnections between the Peruvian central Andes and northeast Brazil during extreme rainfall events in austral summer. J. Hydrometeorol. 17 (2), 499–515. https://doi.org/10.1175/JHM-D-15-0034.1.

Taschetto, A.S., Ummenhofer, C.C., Stuecker, M.F., Dommenget, D., Ashok, K., Rodrigues, R.R., Yeh, S.-W., 2020. ENSO atmospheric teleconnections. In: En El Niño Southern Oscillation in a Changing Climate. American Geophysical Union (AGU), pp. 309–335. https://doi.org/10.1002/9781119548164.ch14.

Tokinaga, H., Richter, I., Kosaka, Y., 2019. ENSO influence on the atlantic Niño, revisited: multi-year versus single-year ENSO events. J. Clim. 32 (14), 4585–4600. https://doi.org/10.1175/JCLI-D-18-0683.1.

UNEP, 1996. Diagnostico Ambiental del Sistema Titicaca-Desaguadero-Poopo-Salar de Coipasa (Sistema TDPS) Bolivia – Perú. United Nations Environment Programme (UNEP), Washington, D.C. (in Spanish).

Vera, C., Higgins, W., Amador, J., Ambrizzi, T., Garreaud, R., Gochis, D., Gutzler, D., Lettenmaier, D., Marengo, J., Mechoso, C.R., Nogues-Paegle, J., Dias, P.L.S., Zhang, C., 2006. Toward a unified view of the American monsoon systems. J. Clim. 19 (20), 4977–5000. https://doi.org/10.1175/JCLI3896.1.

Wang, B., Sun, W., Jin, C., Luo, X., Yang, Y.-M., Li, T., Xiang, B., McPhaden, M.J., Cane, M.A., Jin, F., Liu, F., Liu, J., 2023. Understanding the recent increase in multiyear La Niñas. Nat. Clim. Change 13 (10). https://doi.org/10.1038/s41558-023-01801-6. Article 10.

Wongchuig, S., Carlo Espinoza, J., Condom, T., Junquas, C., Sierra, J.P., Fita, L., Sörensson, A., Polcher, J., 2023. Changes in the surface and atmospheric water budget due to projected Amazon deforestation: lessons from a fully coupled model simulation. J. Hydrol. 625, 130082 https://doi.org/10.1016/j.jhydrol.2023.130082.

Yoon, J.-H., Zeng, N., 2010. An Atlantic influence on Amazon rainfall. Clim. Dynam. 34 (2), 249–264. https://doi.org/10.1007/s00382-009-0551-6.

Zanin, P.R., Satyamurty, P., 2020. Hydrological processes interconnecting the two largest watersheds of South America from multi-decadal to inter-annual time scales: A critical review. Int. J. Climatol. 40, 4006–4038. https://doi.org/10.1002/joc.6442.

Zubieta, R., Molina-Carpio, J., Laqui, W., Sulca, J., Ilbay, M., 2021. Comparative analysis of climate change impacts on meteorological, hydrological, and agricultural droughts in the Lake Titicaca basin. Water 13 (2), 2. https://doi.org/10.3390/w13020175.